

## Modeling and Nonlinear Control of Fuel Cell / Supercapacitor Hybrid Energy Storage System for Electric Vehicles

El Fadil, Hassan; Giri, Fouad; Guerrero, Josep M.; Tahri , Abdelouahad

*Published in:*  
I E E E Transactions on Vehicular Technology

*DOI (link to publication from Publisher):*  
[10.1109/TVT.2014.2323181](https://doi.org/10.1109/TVT.2014.2323181)

*Publication date:*  
2014

*Document Version*  
Early version, also known as pre-print

[Link to publication from Aalborg University](#)

*Citation for published version (APA):*  
El Fadil, H., Giri, F., Guerrero, J. M., & Tahri , A. (2014). Modeling and Nonlinear Control of Fuel Cell / Supercapacitor Hybrid Energy Storage System for Electric Vehicles. *I E E E Transactions on Vehicular Technology*, 63(7), 3011-3018. <https://doi.org/10.1109/TVT.2014.2323181>

### General rights

Copyright and moral rights for the publications made accessible in the public portal are retained by the authors and/or other copyright owners and it is a condition of accessing publications that users recognise and abide by the legal requirements associated with these rights.

- Users may download and print one copy of any publication from the public portal for the purpose of private study or research.
- You may not further distribute the material or use it for any profit-making activity or commercial gain
- You may freely distribute the URL identifying the publication in the public portal -

### Take down policy

If you believe that this document breaches copyright please contact us at [vbn@aub.aau.dk](mailto:vbn@aub.aau.dk) providing details, and we will remove access to the work immediately and investigate your claim.



# **Modeling and Nonlinear Control of Fuel Cell / Supercapacitor Hybrid Energy Storage System for Electric Vehicles**

Hassan El Fadil, Fouad Giri, *Senior Member IEEE* and Josep M. Guerrero, *Senior Member IEEE*

**Abstract**— Compared to conventional powertrains, hybrid electric vehicles exploit energy production and energy storage systems to achieve improved fuel economy. To maximize such improvement, advanced control strategies are needed for controlling in real-time the amount of energy to be produced and stored. This paper deals with the problem of hybrid energy storage system (HESS) for electric vehicle. The storage system consists of a fuel cell (FC), serving as the main power source, and a supercapacitor (SC), serving as an auxiliary power source. It also contains a power block for energy conversion consisting of a boost converter connected with the main source and a boost-buck converter connected with the auxiliary source. The converters share the same dc bus which is connected to the traction motor through an inverter. These power converters must be controlled in order to meet the following requirements: i) tight dc bus voltage regulation; ii) perfect tracking of SC current to its reference; iii) and asymptotic stability of the closed loop system. A nonlinear controller is developed, on the basis of the system nonlinear model, making use of Lyapunov stability design techniques. The latter accounts for the power converters large-signal dynamics as well as for the fuel-cell nonlinear characteristics. It is demonstrated using both a formal analysis and numerical simulations that the developed controller meets all desired objectives.

**Index Terms**—Nonlinear control, electric vehicle, fuel cell, supercapacitor, DC-DC power converters.

## **I. INTRODUCTION**

OIL crisis and environmental issues is enforcing energy technology changes in vehicle manufacturers. Nowadays, further research are being conducted on technologies for the vehicles of the future. Among these technologies the hybrid electric vehicle (HEV) is an efficient and promising perspective [1], [2]. Currently, most hybrid electric vehicles involve

two energy storage devices: one with high energy storage capability, called “Main Energy System” (MES), and the other with high power capability and reversibility, called “Auxiliary Energy System” (AES). The MES provides extended driving range and the AES good acceleration and regenerative braking. Accordingly, fuel cell hybrid electric vehicles (FCHEV) have the potential to improve significantly the fuel economy and can be more efficient than traditional internal combustion engines [3], [4], [5]. The development and infrastructure of FC technologies have been progressing rapidly toward the improvement of the overall system efficiency under realistic automotive loads, while meeting the demands for dynamic response under transient loads or cold start conditions [6], [7]. Although there are various FC technologies available for use in vehicular systems, according to scientists and vehicle developers, a prime candidate is the proton exchange membrane FC (PEMFC) [8] which features higher power density and lower operating temperatures, compared to other types of FC systems.

A stand-alone FC system integrated into an automotive power train is not always sufficient to provide the load demands of a vehicle [9]. To provide the initial power peak during transients such as start up, acceleration or sudden load changes, but also to take advantage of the regenerative power of an electric vehicle at braking, a supercapacitor (SC) bank is needed in addition to the FC [4], [8], [10], [11]. To ensure the dynamic exchange of energy between the FC unit, the load and the SC modules, various power electronics converter topologies and associated controls can be used [12], [13]. The general system topology is depicted in Fig. 1 which is usually called hybrid energy storage system (HESS).

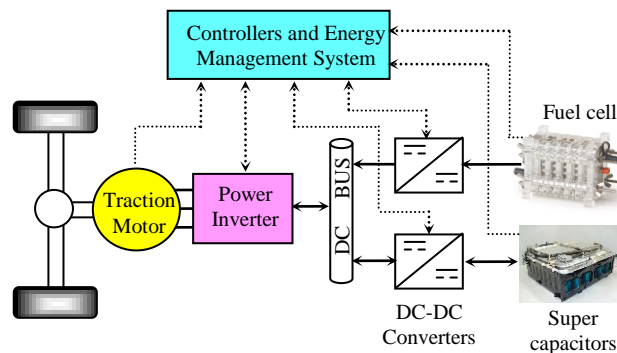


Fig. 1: Power circuit of a typical hybrid vehicle

So far, the problem of controlling the HESS has been dealt with mainly using conventional linear control techniques (see e.g. [14]-[19]). However, it is well established that most dc-dc converters and all fuel cells exhibit strongly nonlinear dynamics [20]. Then, the performances

of any linear controller can only be optimal as long as the system remains around a certain operation point. In this paper, the aim is to investigate the modeling and the control of hybrid energy storage systems taking into account the nonlinear nature of these systems. It will be shown that a quite rigorous nonlinear model can be established and based upon to develop a nonlinear controller using the Lyapunov stability approach. The control objectives are threefold: i) tight dc bus voltage regulation; ii) perfect tracking of SC current to its reference; iii) and asymptotic stability of the closed loop system. It is formally proved that the developed controller does meet its performances. This result is confirmed by several numerical simulations.

The paper is organized as follows. In Section II, the HESS in electric vehicle is described. Sections III is devoted to the system modeling. Controller design and closed-loop analysis is presented in Section IV. The numerical simulation results are presented in Section V. Section VI provides the conclusion of the paper.

## **II. ELECTRIC CIRCUIT STRUCTURE**

Fig. 2 shows the most used hybrid energy storage system (HESS) for electric vehicles [13], [14], [17], [24], [31], [32], [33]. It consists of a 400-V dc link supplied by a 48kW PEMFC used as the main source, through a current nonreversible dc/dc boost converter, a SC bank used as an auxiliary source which is connected to the dc link through a current reversible dc/dc boost-buck converter, and the load constituted of an inverter driving the electric motor. The function of the FC is to supply mean power to the load, whereas the SC is used as a power source that supplies transient power demand and peak current required during acceleration and deceleration stages.

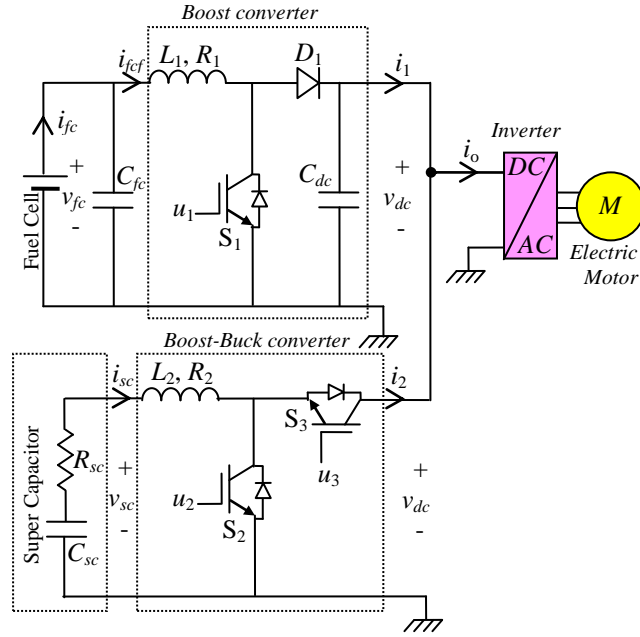


Fig. 2: Fuel cell/supercapacitor hybrid energy storage system

#### A. FC converter (boost)

As the main FC source is not current reversible, the boost power converter is used to adapt the low dc voltage delivered by the FC at rated power of dc bus [14]. The power converter is composed of a high frequency inductor  $L_1$ , an output filtering capacitor  $C_{dc}$ , a diode  $D_1$  and a main IGBT (insulated-gate bipolar transistor) switch  $S_1$  controlled by a binary input signal  $u_1$ . The input capacitor  $C_{fc}$  is used to protect the FC against overvoltage in transient high power demand of the load.

#### B. SC converter (boost-buck)

The SC is connected to the dc bus by means of a two-quadrant dc/dc converter, also called boost-buck converter. The SC current, flowing across the storage device, can be positive or negative allowing energy to be transferred in both directions. The inductor  $L_2$  is used for energy transfer and filtering. Classically, the inductor size is defined by switching frequency and current ripple [21]. The converter is driven by means of binary input signals  $u_2$  and  $u_3$  applied on the gates of the two IGBTs  $S_2$  and  $S_3$ , respectively.

#### C. Energy management strategy of hybrid power source

The main strategy of energy management in combined systems is reported in several works ([21], [22], [23], [24]) and summarizes as follows:

- 1) During low power demand periods, the FC system generates up to its load limit, and the excess power is used to charge the SC. The charging or discharging of the SC bank occurs according to the terminal voltage of the overall load requirements.
- 2) During high power demand periods, the FC system generates the rated power and the SC is discharged to meet the extra power requirements that cannot be supplied by the FC system.
- 3) Short-time power interruptions in the FC system can only be supplied by the SC bank.
- 4) The state of charge of SC bank has to be controlled in order to avoid overcharge or undercharge conditions.
- 5) About 75% of the initial energy stored in the SC bank can be utilized if the terminal load voltage is allowed to decrease to 50% of its initial value. This means that, the energy management system may operate so that, nearly 75% of the initial energy stored in the SC bank can be utilized to compensate transient dc voltage decreases of about 50% of its nominal value.

The practical implementation of the above energy-management strategy entails a proper control of the dc-dc power converters. Accordingly, the boost converter must be driven to realize a classical dc bus voltage regulation. The boost-buck converter must be controlled so that the SC current  $i_{sc}$  tracks well its reference  $I_{scref}$  generated by the energy management system. The generation of  $I_{scref}$  itself is not in the scope of this work, here the emphasis is made on nonlinear control design of the power converters. Let us only notice that the reference current  $I_{scref}$  is positive in discharging mode and negative in charging mode [14].

### **III. SYSTEM MODELING**

The aim of this Subsection is to develop a large-signal model of the power circuit of the energy storage system taking into account their nonlinearities. The developed model will be used later in control design.

#### **A. Energy sources models**

A typical static V-I polarization curve for a single-cell fuel cell is shown in Fig. 3, where the drop of the fuel cell voltage with load current density can be observed. This voltage reduction is caused by three major losses [25]: activation losses, ohmic losses, and transport losses. The V-I polarization curve of Fig. 3 corresponds to a Ballard manufacturer elementary FC 1020ACS.

The SC can be represented by its classical equivalent circuit consisting of a capacitance ( $C_{sc}$ ), an equivalent series resistance (ESR,  $R_{sc}$ ) representing the charging and discharging resistance and an equivalent parallel resistance (EPR) representing the self discharging losses [26]. The EPR models the leakage effects, which only impacts the long term energy storage performance of the SC [27], thus it is omitted in this paper. The focus will then be put on power converters modeling.

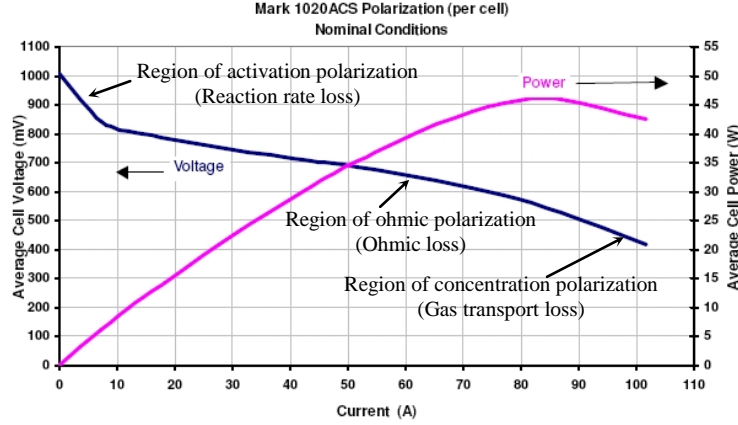


Fig. 3: V-I characteristic of elementary single cell of the PEMFC made by Ballard

### B. Boost converter modeling

From Fig. 2 one can obtain the power stage bilinear equations, considering some non-idealities. For instance, the inductances  $L_1$  and  $L_2$  shown in Fig. 2 involve equivalent series resistances (ESR), respectively denoted  $R_1$  and  $R_2$ . Each IGBT switch is controlled by using a PWM signal  $u_j$  ( $j=1,2,3$ ) which takes values in the set  $\{0, 1\}$ . The inspection of the circuit shown in Fig. 2 leads to the following bilinear switching model:

$$\frac{di_{fcf}}{dt} = -(1-u_1) \frac{v_{dc}}{L_1} - \frac{R_1}{L_1} i_{fcf} + \frac{v_{fc}}{L_1} \quad (1a)$$

$$\frac{dv_{dc}}{dt} = (1-u_1) \frac{i_{fcf}}{C_{dc}} - \frac{1}{C_{dc}} i_1 \quad (1b)$$

where  $i_{fcf}$  and  $i_1$  are respectively the inductor input current and the output current of the boost converter;  $v_{fc}$  is the FC voltage and  $v_{dc}$  the dc bus voltage.

### C. Boost-buck converter modeling

This converter operates as a boost converter or a buck converter. Indeed, in discharging



mode ( $i_{sc} > 0$ ) the converter operates as a boost converter, and in charging mode ( $i_{sc} < 0$ ) it operates as a buck converter. As the goal is to enforce the SC current  $i_{sc}$  to track its reference  $i_{scref}$  (provided by the energy management system), one can define a binary variable  $k$  as follows:

$$k = \begin{cases} 1 & \text{if } i_{scref} > 0 \quad (\text{Boost mode}) \\ 0 & \text{if } i_{scref} < 0 \quad (\text{Buck mode}) \end{cases} \quad (2)$$

#### 1) Boost mode operation ( $k=1$ )

In this case the control input signal  $u_3$  is fixed to zero ( $u_3=0$ ) and  $u_2$  is a PWM variable input. From inspection of the circuit, shown in Fig. 2 and taking into account that  $u_2$  can take the binary values 1 or 0, the following bilinear switching model can be obtained:

$$\frac{di_{sc}}{dt} = -(1-u_2) \frac{v_{dc}}{L_2} - \frac{R_2}{L_2} i_{sc} + \frac{v_{sc}}{L_2} \quad (3a)$$

$$i_2 = (1-u_2)i_{sc} \quad (3b)$$

where  $i_{sc}$  is the SC current.

#### 2) Buck mode ( $k=0$ )

The control input signal  $u_2$  is fixed to zero ( $u_2=0$ ) and  $u_3$  acts as the PWM variable input. Also, from Fig. 2 and taking in account that  $u_3 \in \{0, 1\}$ , the following model can be obtained

$$\frac{di_{sc}}{dt} = -u_3 \frac{v_{dc}}{L_2} - \frac{R_2}{L_2} i_{sc} + \frac{v_{sc}}{L_2} \quad (4a)$$

$$i_2 = u_3 i_{sc} \quad (4b)$$

### D. Global system modeling

The combination of the previous partial models (1), (3) and (4) leads to a global model representing the whole system. Indeed, combining (3) and (4) one gets the following global model of the boost-buck converter:

$$\frac{di_{sc}}{dt} = -[k(1-u_2) + (1-k)u_3] \frac{v_{dc}}{L_2} - \frac{R_2}{L_2} i_{sc} + \frac{v_{sc}}{L_2} \quad (5a)$$

$$i_2 = [k(1-u_2) + (1-k)u_3]i_{sc} \quad (5b)$$

On the other hand, from Fig. 2 and taking into account (5b), one has:

$$i_1 = i_o - i_2 = i_o - [k(1-u_2) + (1-k)u_3]i_{sc} \quad (6)$$

where  $i_o$  is the load current. Finally, using (1), (5a) and (6), the following bilinear switched model of the global system is obtained:

$$\frac{di_{fcf}}{dt} = -(1-u_1)\frac{v_{dc}}{L_1} - \frac{R_1}{L_1}i_{fcf} + \frac{v_{fc}}{L_1} \quad (7a)$$

$$\frac{di_{sc}}{dt} = -u_{23}\frac{v_{dc}}{L_2} - \frac{R_2}{L_2}i_{sc} + \frac{v_{sc}}{L_2} \quad (7b)$$

$$\frac{dv_{dc}}{dt} = (1-u_1)\frac{i_{fcf}}{C_{dc}} + u_{23}\frac{i_{sc}}{C_{dc}} - \frac{i_o}{C_{dc}} \quad (7c)$$

where  $u_{23}$  stands as a 'virtual' control input variable of the boost-buck converter and is defined as follows:

$$u_{23} = k(1-u_2) + (1-k)u_3 \quad (8)$$

The question of how getting the actual control signals  $u_2$  and  $u_3$  from  $u_{23}$  will be investigated later in this paper. For control design purpose, it is more convenient to consider the following averaged model, obtained by averaging the model (7) over the switching periods:

$$\frac{dx_1}{dt} = -(1-\mu_1)\frac{x_3}{L_1} - \frac{R_1}{L_1}x_1 + \frac{v_{fc}}{L_1} \quad (9a)$$

$$\frac{dx_2}{dt} = -\mu_{23}\frac{x_3}{L_2} - \frac{R_2}{L_2}x_2 + \frac{v_{sc}}{L_2} \quad (9b)$$

$$\frac{dx_3}{dt} = (1-\mu_1)\frac{x_1}{C_{dc}} + \mu_{23}\frac{x_2}{C_{dc}} - \frac{i_o}{C_{dc}} \quad (9c)$$

where  $x_1$  represents the average value of the current  $i_{fcf}$  ( $x_1 = \langle i_{fcf} \rangle$ ),  $x_2$  the average value of the SC current ( $x_2 = \langle i_{sc} \rangle$ ),  $x_3$  the average value of the dc bus voltage  $v_{dc}$  ( $x_3 = \langle v_{dc} \rangle$ ),  $\mu_1$  and  $\mu_{23}$  the duty cycles, i.e. average values of the binary control inputs  $u_1$  and  $u_{23}$  ( $\mu_1 = \langle u_1 \rangle$ ,  $\mu_{23} = \langle u_{23} \rangle$ ). By definition, the duty cycles take their values in the interval  $[0,1]$ . Notice that the nonlinear model (9) is a multi-input multi-output (MIMO) system, which increases the complexity of the control problem.

#### IV. CONTROLLER DESIGN AND ANALYSIS

This Section is devoted to the design and the analysis of an appropriate controller based on the MIMO nonlinear system model (9).

##### A. Control objectives

We are seeking a controller able to achieve the following control objectives:

- i) ensuring tight dc bus voltage regulation under load variations,
- ii) enforcing the SC current  $i_{sc}$  to track well its reference  $i_{scref}$ ,
- iii) and guaranteeing asymptotic stability of the whole energy system.

##### B. Nonlinear control design

Once the control objectives are defined, as the MIMO system is highly nonlinear, a Lyapunov based nonlinear control is proposed [30]. The first control objective is to enforce the dc bus voltage  $v_{dc}$  to track a given constant reference signal  $V_{dcref}$ . In this respect, recall that the boost converter has a non-minimum phase feature [28], [29]. Such an issue is generally dealt with by resorting to an indirect design strategy. More specifically, the objective is to enforce the input inductor current  $i_{fcf}$  to track a reference signal, i.e.  $I_{fcfref}$ . The latter is chosen so that if (in steady state)  $i_{fcf} = I_{fcfref}$  then,  $v_{dc} = V_{dcref}$  where  $V_{dcref} > v_{fc}$ . It follows from power conservation considerations, also called PIPO (Power Input equals Power Output), that  $I_{fcfref}$  is related to  $V_{dcref}$  by means of the following relationship

$$I_{fcfref} = \lambda \left( \frac{V_{dcref} i_o - v_{sc} I_{scref}}{v_{fc}} \right) \quad (10)$$

where  $\lambda \geq 1$  is an ideality factor introduced to take into account all losses: switching losses in the converters and the losses in the inductances ESR ( $R_1$  and  $R_2$ ). To carry out the first control objective, the following error is defined

$$e_1 = x_1 - I_{fc\text{ref}} \quad (11)$$

Achieving the dc bus voltage regulation objective entails the regulation of the error  $e_1$  at zero.

To this end, the dynamic of  $e_1$  has to be identified. Deriving (11), one gets using (9a):

$$\dot{e}_1 = -(1 - \mu_1) \frac{x_3}{L_1} - \frac{R_1}{L_1} x_1 + \frac{v_{fc}}{L_1} - \dot{I}_{fc\text{ref}} \quad (12)$$

To make  $e_1$  exponentially vanish amounts to enforcing  $\dot{e}_1$  to behave as follows:

$$\dot{e}_1 = -c_1 e_1 + e_3 \quad (13)$$

where  $c_1 > 0$  is a design parameter and

$$e_3 = x_3 - x_{3d} \quad (14)$$

is the error between the dc bus voltage  $x_3$  and  $x_{3d}$  is its desired value to be defined later.

Comparing (12) and (13) one gets the control law of the boost converter control signal:

$$\mu_1 = 1 - \frac{L_1}{x_3} \left\{ c_1 e_1 - e_3 + \frac{v_{fc} - R_1 x_1}{L_1} - \dot{I}_{fc\text{ref}} \right\} \quad (15)$$

In (15),  $e_3$  is a damping term introduced in the control law to adjust the output response. Its dynamic will be investigated later.

The next step is to elaborate a control law for the boost-buck converter input signal  $\mu_{23}$ , bearing in mind the second control objective. To this end, the following error is introduced

$$e_2 = x_2 - I_{sc\text{ref}} \quad (16)$$

The time-derivation of (16) yields, using (9b):

$$\dot{e}_2 = -\mu_{23} \frac{x_3}{L_2} - \frac{R_2}{L_2} x_2 + \frac{v_{sc}}{L_2} - \dot{i}_{scref} \quad (17)$$

The achievement of the tracking objective regarding the SC current  $i_{sc}$  amounts to enforcing the error  $e_2$  to decrease, if possible exponentially. One possible way is to let  $e_2$  undergo following differential equation:

$$\dot{e}_2 = -c_2 e_2 \quad (18)$$

where  $c_2 > 0$  is a design parameter. Finally, from (16) and (18), the control law  $\mu_{23}$  can be easily obtained as follows

$$\mu_{23} = \frac{L_2}{x_3} \left\{ c_2 e_2 + \frac{v_{sc} - R_2 x_2}{L_2} - \dot{i}_{scref} \right\} \quad (19)$$

Now that the control laws generating  $\mu_1$  and  $\mu_{23}$  are defined, respectively by (15) and (19), the concern is to check that the stability of the closed loop is guaranteed. This is performed in the next Subsection.

### **C. Stability analysis**

The third control objective, i.e. closed-loop stability, will now be analyzed. This is carried out by checking that the control laws (15) and (19) stabilize the error system with state variables  $(e_1, e_2, e_3)$ . To this end, the following quadratic Lyapunov function is considered:

$$V = \frac{1}{2} e_1^2 + \frac{1}{2} e_2^2 + \frac{1}{2} e_3^2 \quad (20)$$

Recall that, at this point, the signal  $x_{3d}$  (the desired value of the dc bus voltage  $x_3$  used in the control law (15)) is still not defined. The key idea is to select  $x_{3d}$  so that the time-derivative  $\dot{V}$  is made negative definite. That derivative is readily obtained from (20), using (13) and (18):

$$\dot{V} = -c_1 e_1^2 - c_2 e_2^2 + e_3 (e_1 + \dot{e}_3) \quad (21)$$

This suggests that the derivative  $\dot{e}_3$  is made time-varying according to the following differential equation:

$$\dot{e}_3 = -c_3 e_3 - e_1 \quad (22)$$

where  $c_3 > 0$  being a design parameter. Indeed, if (22) holds then (21) simplifies to:

$$\dot{V} = -c_1 e_1^2 - c_2 e_2^2 - c_3 e_3^2 \quad (23)$$

Then,  $\dot{V}$  will actually be negative definite which entails the global asymptotic stability of the equilibrium  $(e_1, e_2, e_3) = (0, 0, 0)$ . Now, for equation (22) to hold, it follows from (14) and (9c) that the signal  $x_{3d}$  must be generated according to the following law:

$$\dot{x}_{3d} = \frac{1}{C_{dc}} [(1 - \mu_1)x_1 + \mu_{23}x_2 - i_o] + c_3 e_3 + e_1 \quad (24)$$

or, equivalently:

$$x_{3d} = \frac{1}{s} \left\{ \frac{1}{C_{dc}} [(1 - \mu_1)x_1 + \mu_{23}x_2 - i_o] + c_3 e_3 + e_1 \right\} \quad (25)$$

where  $s$  denotes the Laplace operator. The main results of the paper are now summarized in the following theorem.

**Theorem.** Consider the closed-loop system consisting of the fuel cell supercapacitor hybrid energy storage system represented by (7a-c), and the controller composed by the control laws (15) and (19). Then, one has:

- i) The error system with state variables  $(e_1, e_2, e_3)$  is GAS around the origin  $(0, 0, 0)$ .
- ii) The error  $e_1$  converge asymptotically to zero implying tight dc bus voltage regulation.
- iii) The error  $e_2$  converge asymptotically to zero implying perfect tracking of SC current  $i_{sc}$  to its reference  $i_{scref}$   $\square$

**Proof. Part i.** From (20) and (23) one has  $V$  positive definite and  $\dot{V}$  negative definite which implies that the closed loop system with the state vector  $(e_1, e_2, e_3)$  is globally asymptotically

stable (GAS).

**Part ii.** Equation (21) can be rewritten as follows:  $\dot{V} \leq -2\beta V$ , where  $\beta = \min(c_1, c_2, c_3)$ .

Hence,  $V$  trends to be zero exponentially fast, which in turn means that, using (20), the errors  $e_1, e_2$  and  $e_3$  are exponentially vanishing. The vanishing of the error  $e_1$  implies, using (11) and (10), the convergence of the steady-state error  $x_2 - V_d$  to zero. This, indeed, implies a tight dc bus voltage regulation.

**Part iii.** The vanishing of the error  $e_2$  implies, using (16), that the SC current  $i_{sc}$  perfectly tracks its reference  $i_{scref}$ . This ends the proof of Theorem ■

**Remark 1.** The results of this theorem are independent on the nature and characteristics of the involved vehicle motor. The latter may be any AC (induction, PM synchronous,...) or DC motor. The only important fact is that the load current  $i_o$  must be accessible to measurements. However, different components of the system (motor, energy storage system, control parameters...) must be selected taking into account the considered type vehicle. In particular, the vehicle mass and its operation conditions determine the possible convenient traction motors. This aspect is widely discussed in existing references (e.g. [1], [2], [11], [34], [35]), but is not in the scope of the present study.

## V. SIMULATION RESULTS

The performances of the developed nonlinear controller will now be illustrated using numerical simulations.

### A. System characteristics

The simulations are performed considering a vehicle with the following specifications: Acceleration 0-100 km/h in 12.5sec on ground level; vehicle mass (including mass of vehicle, energy storage system and power converters) 1922 kg; rolling resistance coefficient 0.01; aerodynamic drag coefficient 0.3; front area 2.5 m<sup>2</sup>; maximum speed 120 km/h.

The traction induction motor has the following characteristics: nominal power of 45kW and a peak of 75kW; maximum speed of 3500 rpm; maximum torque of 255Nm.

The PEMFC has the following characteristics: nominal voltage of 200V; nominal current of 200A; maximum power of 48kW. The FC static characteristic is plotted in Fig. 4.

The supercapacitor module consists of two blocks in parallel. Each block contains 141 cells of supercapacitors connected in series. The single supercapacitor cell had a minimal capacitance

of 1500 F and a nominal voltage of 2.5 V. The cells have a maximum specific energy of 5.3Wh/kg and a maximum specific power of 4.8kW/kg.

The simulation bench of the hybrid energy storage system control is described by Fig. 5 and is simulated using the MATLAB software. Its power part is illustrated by Fig. 6 and the corresponding parameters have the numerical values of Table 2. Fig. 7 shows the circuit which generates the binary input signals  $u_2$  and  $u_3$ , of the boost-buck converter, from the control law  $\mu_{23}$  and  $i_{scref}$  according to equations (2) and (8).

TABLE 2: PARAMETERS OF THE CONTROLLED SYSTEM

Parameter	Value
Inductance $L_1$ and $L_2$	3.3mH
Inductances ESR, $R_1$ and $R_2$	20m $\Omega$
DC bus Filtering capacitor, $C_{dc}$	1.66mF
Boost input capacitor, $C_{fc}$	1.66mF
Supercapacitor, $C_{sc}$	21.27F
Supercapacitor ESR, $R_{sc}$	66m $\Omega$
Switching frequency, $f_s$	15kHz

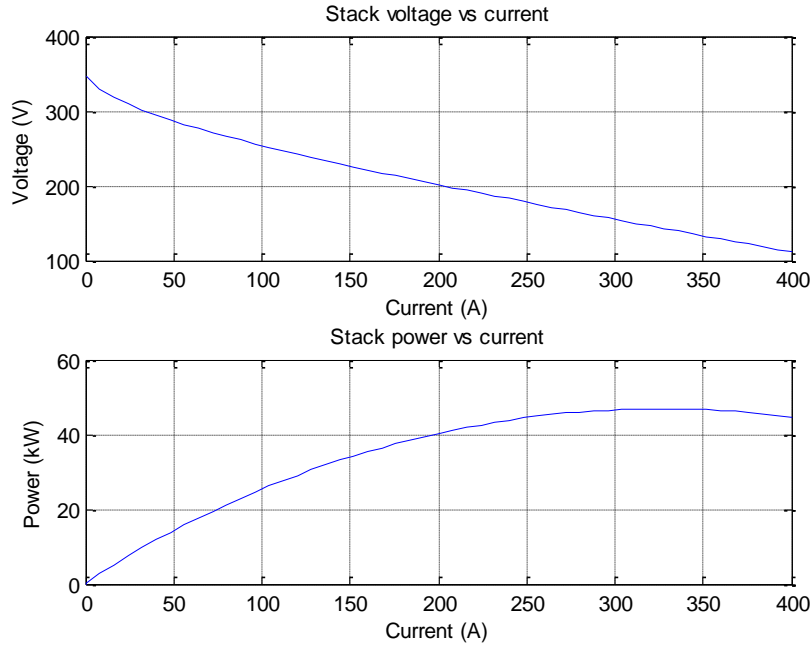


Fig. 4: V-I and P-I characteristics of used PEMFC



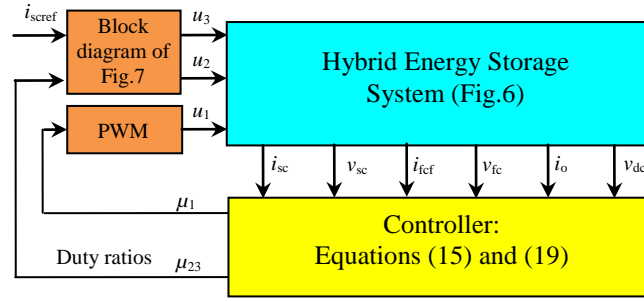


Fig. 5: Simulation bench for the HESS control

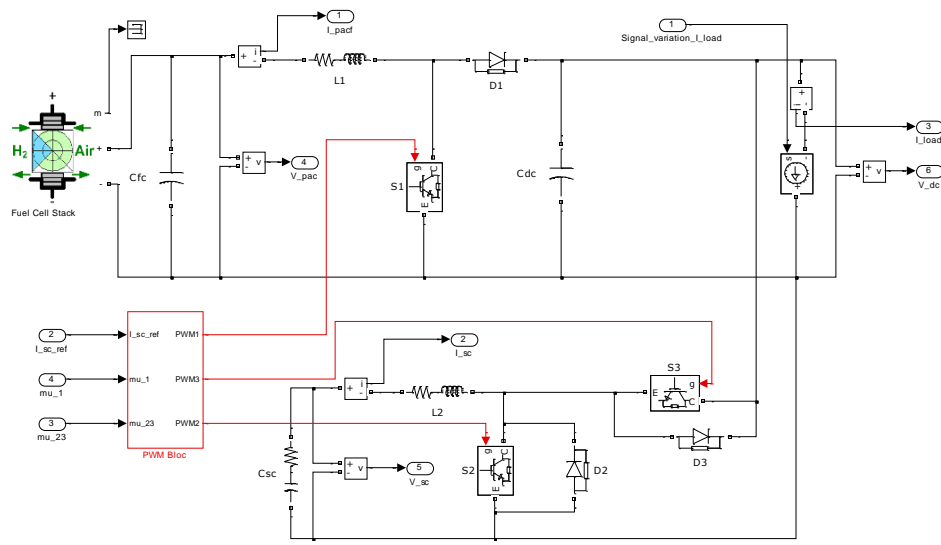


Fig.6: Power part of the HESS by using Power Systems Toolbox of Matlab-Simulink

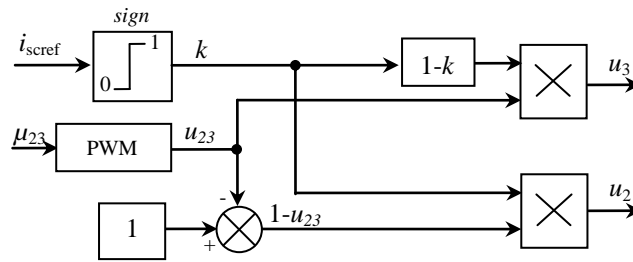


Fig. 7: Block diagram of input signals  $u_2$  and  $u_3$  generation

The control design parameters are given the following numerical values which have proved to be convenient:  $c_1 = 10^3$ ,  $c_2 = 10^3$  and  $c_3 = 10^2$ . The ideality factor used in equation (10) is  $\lambda = 1.015$ .

**Remark 2.** Theoretically, the design parameters  $c_1$ ,  $c_2$  and  $c_3$  must only be positive. But, the

achieved transient performances are determined by these values. The point is that (and this is generally the case in nonlinear control design), there is no systematic rule for conveniently selecting these numerical values. The usual practice is to use the try-error method which consists in progressively increasing the parameter values until a satisfactory compromise is achieved between rapidity of responses and control activity.

### ***B. Tracking capability of the proposed controllers***

In this Subsection, the objective is to check the tracking behavior of the proposed controller. The resulting control performances are shown by Figs 8 to 15. Fig. 8 to 11 describe the controller performances in presence of a constant reference  $I_{scref} = 10A$  and successive load current ( $i_o$ ) jumps. The jumps occur between 50A and 20A, and between 20A and 70A. Notice that the control performances are satisfactory, despite the load current variations. Indeed, Fig. 8 shows that the dc voltage  $v_{dc}$  is well regulated to its desired value  $V_{dcref} = 400V$ . Fig. 9 illustrates that the Sc current  $i_{sc}$  tracks well its reference and that the SC is in discharging mode. The FC signals  $v_{fc}$  and  $i_{fc}$  are shown in Fig. 10. Finally, Fig. 11 illustrates the control signals  $\mu_1$  and  $\mu_{23}$ .

Figures 12 to 15 describe the controller performances in presence of a constant current load ( $i_o = 40A$ ) and successive variations of the SC current reference  $I_{scref}$ . The variations are performed with current changes from 20A to  $-30A$ , and from  $-30A$  to 10A. Also, figures show that the control behavior is satisfactory. Indeed, Fig. 12 shows that the dc voltage  $v_{dc}$  is perfectly regulated to its desired value  $V_{dcref} = 400V$ . Fig. 13 illustrates that the SC current  $i_{sc}$  tracks its reference signal  $I_{scref}$ . Finally, the FC signals and the control signals are shown in Figs 14 and 15, respectively.

### ***C. Controllers behavior in presence of a driving cycle***

The main objective here is to illustrate the controller performances under the European EUDC (Extra Urban Driving Cycle) driving cycle. The latest constitutes a real test to assess the effectiveness of the proposed controllers in automotive applications. Accordingly, Fig. 16 shows a speed profile while Fig.17 illustrates the corresponding load power  $P_0$  and the load current  $i_o$ . Assuming that the system consisting of the induction motor and the inverter is operating with an efficiency of 75% and that the dc bus voltage is regulated to its desired

value  $V_{dcref} = 400V$ , the load power and the load current are obtained, from the vehicle speed, as follows [36]:

$$P_0 = 1.33 \left\{ \frac{1}{2} \rho_{air} v_t^2 S C_x + M_t g C_r + M_t \frac{dv_t}{dt} \right\} v_t \quad (26)$$

$$i_0 = \frac{1.33}{400} \left\{ \frac{1}{2} \rho_{air} v_t^2 S C_x + M_t g C_r + M_t \frac{dv_t}{dt} \right\} v_t \quad (27)$$

where  $v_t$  denotes the vehicle speed;  $M_t$  the total mass of the vehicle;  $C_x$  the aerodynamic drag coefficient;  $S$  the front area;  $C_r$  the rolling resistance coefficient;  $g$  the gravitational acceleration constant, and  $\rho_{air}$  the air density. Note that the maximum speed of the considered EUDC cycle is 100 km/h.

Fig.18 shows that the dc bus voltage  $v_{dc}$  is regulated to its desired value  $V_{dcref} = 400V$ . Fig. 19 show the SC current and voltage. Clearly, the SC current  $i_{sc}$  tracks well its reference  $i_{scref}$ . The FC voltage  $v_{fc}$  and the FC current  $i_{fef}$  are plotted in Fig. 20. Finally, Fig. 21 illustrates the control signals  $\mu_1$  and  $\mu_{23}$ .

## VI. CONCLUSION

The problem of controlling a hybrid energy storage system, used in electric vehicles, has been addressed. The system consists of a PEM fuel cell as the main source and a supercapacitor as the auxiliary source. The energy conversion between the sources and the load is managed using two dc-dc power converters. A controller is developed that generates the binary power converters input signals in order to meet the following requirements: i) tight dc voltage regulation, ii) perfect tracking of supercapacitor current to its reference and, iii) asymptotic stability of the closed loop system. The controller is designed on the basis on the nonlinear averaged model of the system, using Lyapunov stability theory. It is formally shown, using this theory, that the developed control strategy actually meets the control objectives whatever the vehicle and motor type. Interestingly, the only used information on the motor part is the measurement of the load current  $i_0$ .

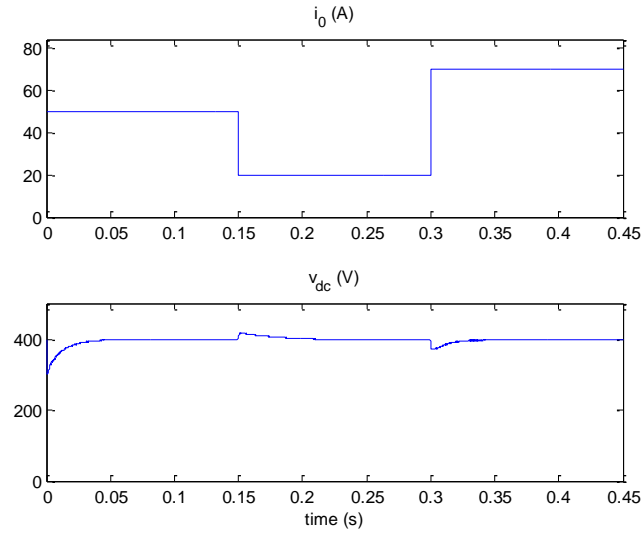


Fig. 8: The dc voltage in presence of load current step-changes

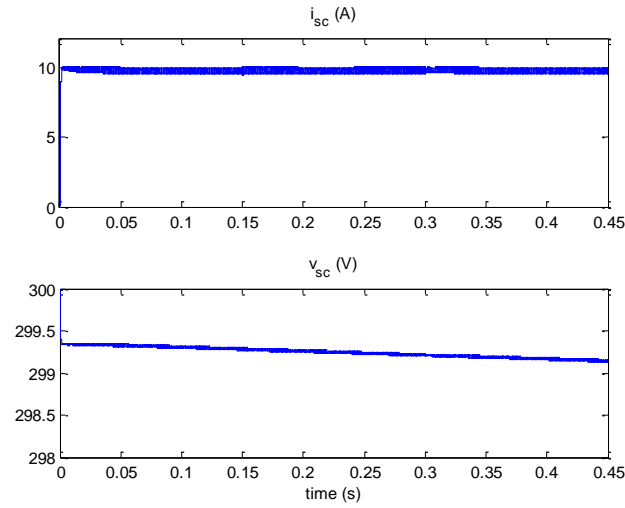


Fig. 9: Current and voltage SC waveforms for the load current step-changes

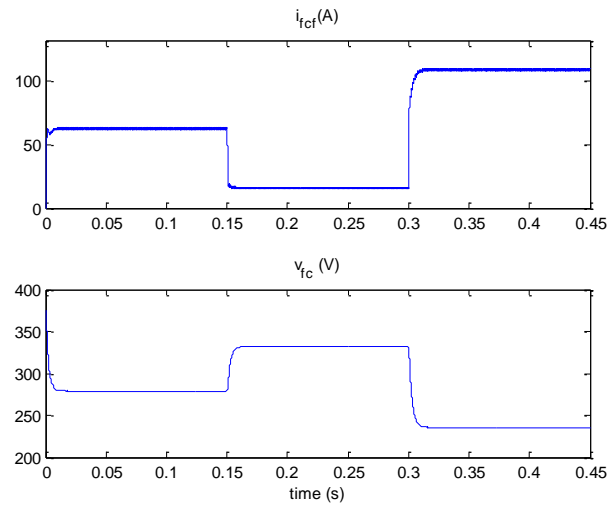


Fig. 10: FC signals for load current step-changes

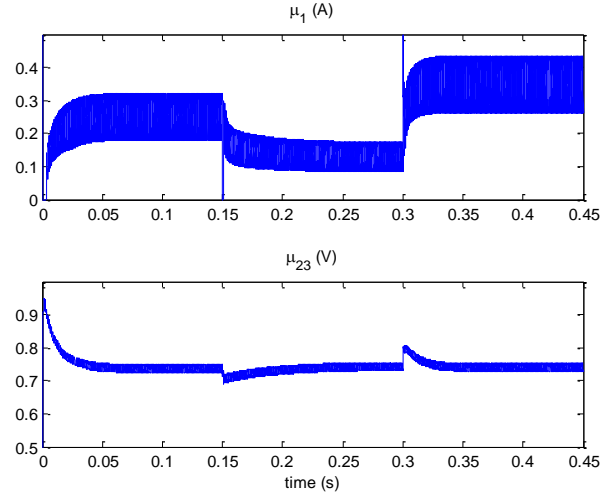


Fig. 11: Control signals  $\mu_1$  and  $\mu_{23}$  for load current step-changes

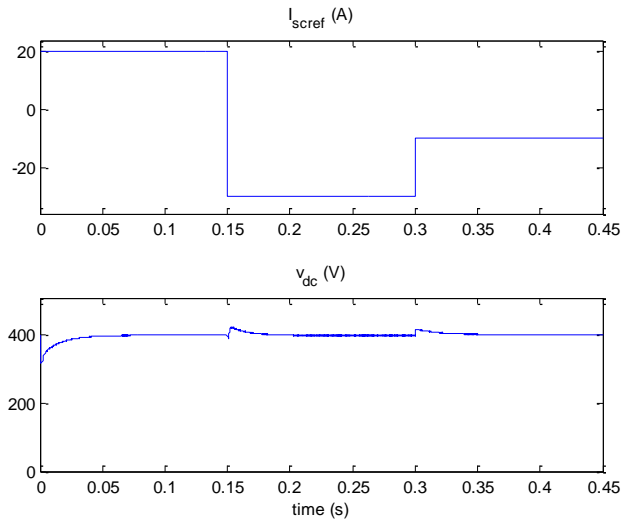


Fig. 12: The dc voltage waveform for SC current reference step-changes

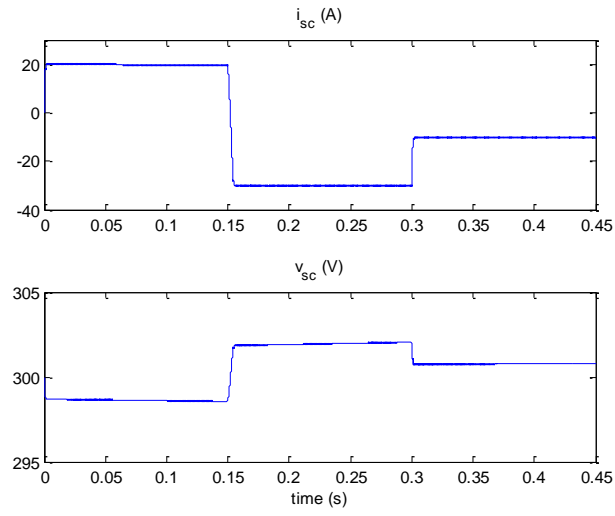


Fig. 13: SC voltage and current waveforms for SC current reference step-changes

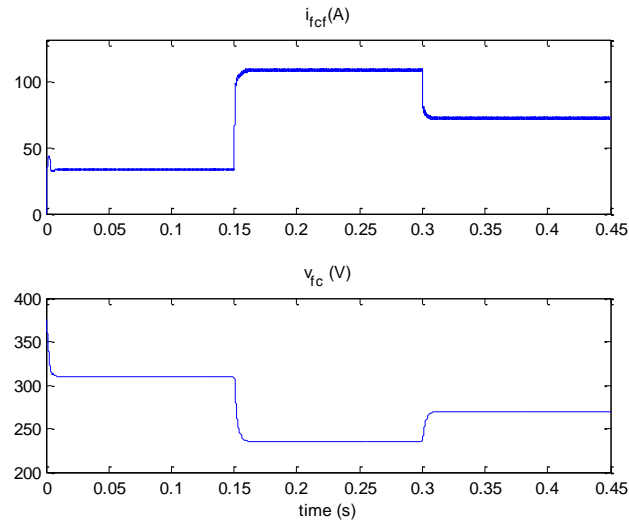


Fig. 14: FC voltage and current for SC current reference step-changes

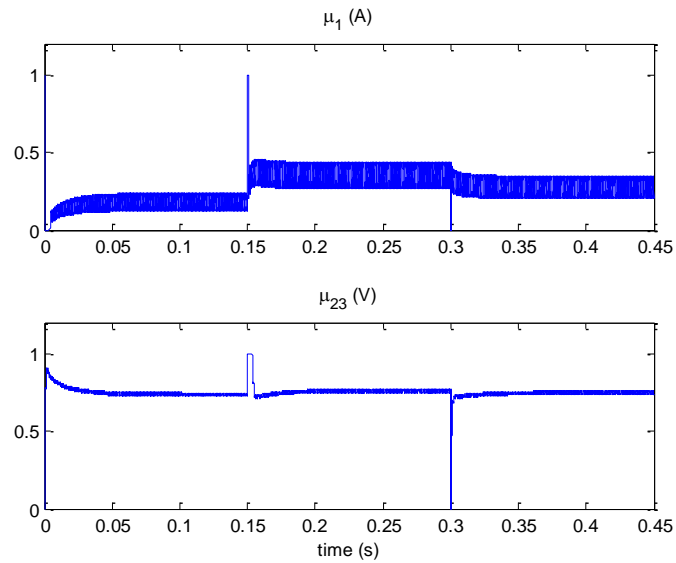


Fig. 15: The control signals in presence of SC current reference jumps

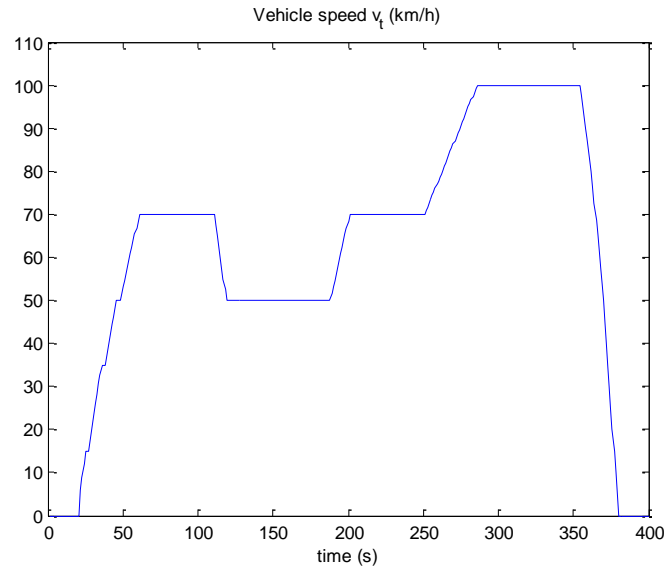


Fig. 16: EUDC driving cycle used for simulations

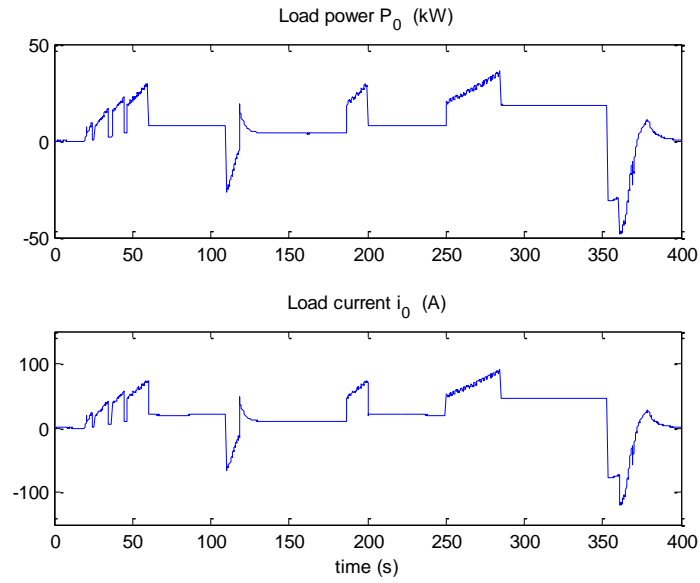


Fig. 17: Load power  $P_0$  and load current  $i_0$  corresponding to the speed profile and vehicle specifications

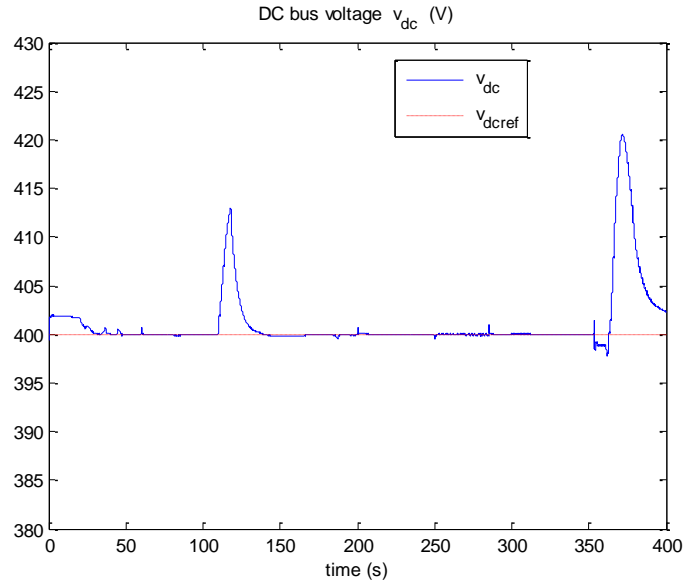


Fig. 18: The dc voltage signal in presence of the EUDC driving cycle

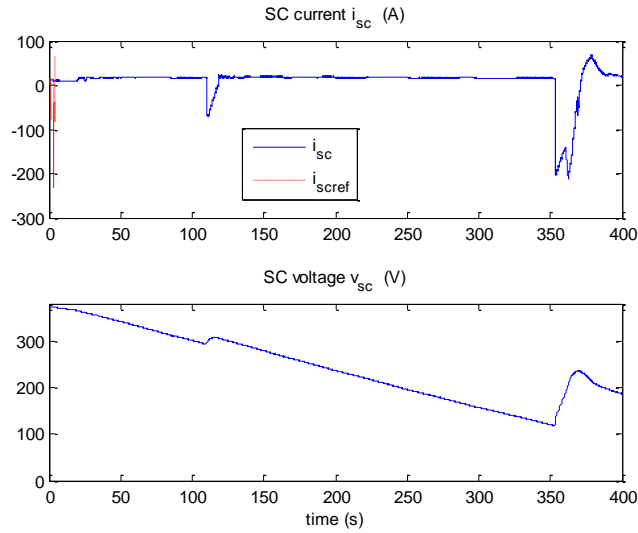


Fig. 19: SC signals (current and voltage) in presence of the EUDC driving cycle



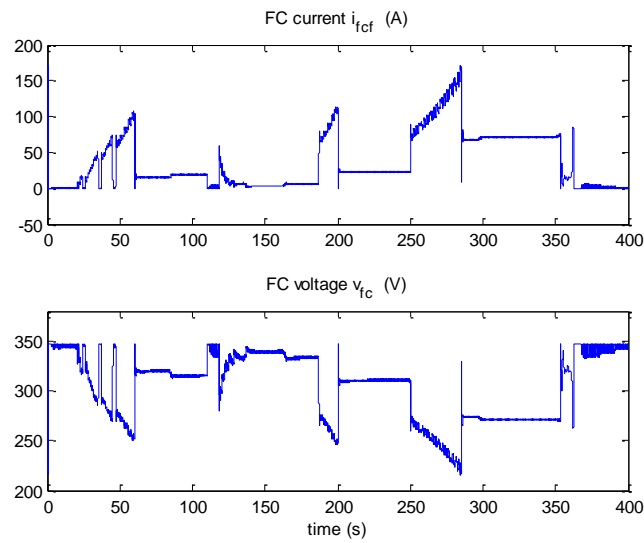


Fig. 20: FC signals (current and voltage) in presence of the EUDC driving cycle

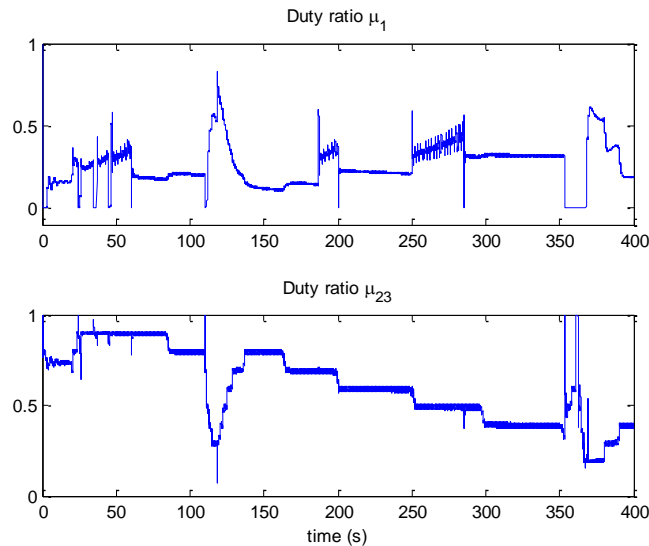


Fig. 21: The control signals in presence of the EUDC driving cycle

## REFERENCES

- [1] C.C. Chan, "The State of the Art of Electric, Hybrid, and Fuel Cell Vehicles", *In proceedings of the IEEE*, vol.95,no.4, pp.704-718, Apr.2007.
- [2] O.D. Momoh, M.O. Omoigui, "An overview of hybrid electric vehicle technology" *In proc. Of IEEE Vehicle Power and Propulsion Conference, VPPC '09.*, Sept. 2009, pp. 1286 – 1292.
- [3] K. Rajashekara . "Hybrid fuel-cell strategies for clean power generation". *IEEE Transactions on Industry Applications*, vol.41, no.3, pp.682 – 689, May 2005.

- [4] J.T. Pukrushpan, H. Peng, and A.G. Stefanopoulou, "Control-oriented modeling and analysis for automotive fuel cell system". *Journal of Dynamic Systems, Measurement, and Control*, vol.126, no.1, pp.14–25, Apr.2004.
- [5] J.T. Pukrushpan, A.G. Stefanopoulou, and H. Peng. *Control of Fuel Cell Power Systems: Principles; Modeling; Analysis and Feedback Design*. Springer, 2005.
- [6] Y. Guezennec, T.Y. Choi, G. Paganelli and G. Rizzoni, "Supervisory control of fuel cell vehicles and its link to overall system efficiency and low level control requirements". *In proc. Of Amer. Cont. Conf.*, 4–6 June 2003, vol.3, pp. 2055–2061.
- [7] C. C. Chan and Y. S. Wong, "Electric vehicles charge forward," *IEEE Power Energy Mag.*, vol. 2, no. 6 , pp. 24–33, Nov./Dec. 2004.
- [8] A. Emadi, K. Rajashekara, S.S. Williamson and S.M. Lukic, "Topological overview of hybrid electric and fuel cell vehicular power system architectures and configurations". *IEEE Trans. Veh. Technol.*, vol.54, no.3, pp.763–70. May 2005.
- [9] D.D. Boettner, G. Paganelli, Y.G. Guezennec, G. Rizzoni and M.J.Moran, "Proton exchange membrane fuel cell system model for automotive vehicle simulation and control". *J. Energy Resour. Technol.* vol.124, no.1, 20-27, Mar. 2002.
- [10] W.F. Powers and P.R. Nicastrì, "Automotive vehicle control challenges in the 21st century". *Control Eng Pract*, vol.8, no.6, pp.605–618., June 2000
- [11] A. Emadi, M. Ehsani and J.M. Miller, *Vehicular electric power systems*. New York: Marcel Dekker Inc., 2004.
- [12] M. B. Burnett and L. J. Borle, "A power system combining batteries and supercapacitors in a solar/hydrogen hybrid electric vehicle," *in Proc. IEEE Conf. Veh. Power Propuls.*, Sep. 7–9, 2005, pp. 711–714.
- [13] A. Khaligh and Li. Zhihao, "Battery, Ultracapacitor, Fuel Cell, and Hybrid Energy Storage Systems for Electric, Hybrid Electric, Fuel Cell, and Plug-In Hybrid Electric Vehicles: State of the Art", *IEEE Transactions on Vehicular Technology*, vol.58, no.6, pp.2806 – 2814, July 2010.
- [14] P. Thounthong, S. Rael and B. Davat, "Control Strategy of Fuel Cell and Supercapacitors Association for a Distributed Generation System", *IEEE Trans. On Indus. Elect.*, vol. 54, no.6, pp.3225 – 3233, Dec. 2007.
- [15] P. Alireza, S. Pierfederici and F. Meibody-Tabar, "Energy control of supercapacitor/fuel cell hybrid power source", *Energy Conversion and Management*, vol.49, no.6, pp.1637–1644, June 2008.
- [16] M. Marchesoni and C. Vacca, "New DC–DC Converter for Energy Storage System Interfacing in Fuel Cell Hybrid Electric Vehicles", *IEEE Trans on Power Elect.*, vol.22, no.1, pp.301-308, Jan. 2007.
- [17] A.S. Samosir and A.H.M. Yatim, "Implementation of Dynamic Evolution Control of Bidirectional DC–DC Converter for Interfacing Ultracapacitor Energy Storage to Fuel-Cell System", *IEEE Trans. On Indus. Elect.*, vol.57, no.10, pp.3468-3473, Feb. 2010.
- [18] M.H.Todorovic, L. Palma and P.N. Enjeti, "Design of a Wide Input Range DC–DC Converter With a Robust Power Control Scheme Suitable for Fuel Cell Power Conversion", *IEEE Trans. On Indus. Elect.*, vol.55, no.3, pp.1247 – 1255, Mar. 2008.
- [19] D. Rotenberg, A. Vahidi, and I. Kolmanovsky, "Ultracapacitor Assisted Powertrains: Modeling, Control, Sizing, and the Impact on Fuel Economy", *IEEE Trans. On Contr. Syst. Tech.*, vol.19, no.3, pp.576 – 589, May 2011.
- [20] H. El Fadil, F. Giri, J.M. Guerrero and B. Salhi, "Adaptive Control of Interleaved Boost Converter for Fuel Cell Energy", *In Proc. Of the IEEE American Control Conference*, Jun 2011, pp. 3905-3910.
- [21] M. Ortúzar, J. Moreno, and J. Dixon, "Ultracapacitor-based auxiliary energy system for an electric vehicle: Implementation and evaluation," *IEEE Trans. Ind. Electron.*, vol. 54, no. 4, pp. 2147–2156, Aug. 2007.
- [22] A. Vahidi, A. Stefanopoulou and P. Huet, "Current Management in a Hybrid Fuel Cell Power System: A Model-Predictive Control Approach", *IEEE Trans. On Contr. Syst. Tech.*, vol.14, no.6, pp.1047 – 1057, Nov. 2006.

- [23] A. Payman, S. Pierfederici and F. Meibody-Tabar, "Energy Management in a Fuel Cell/Supercapacitor Multisource/Multiload Electrical Hybrid System", *IEEE Trans. On Power Elect.*, vol.24, no12, pp.2681 – 2691, Dec. 2009.
- [24] M. Zandi, A. Payman, J.P. Martin, S. Pierfederici, B. Davat and F. Meibody-Tabar, "Energy Management of a Fuel Cell/Supercapacitor/Battery Power Source for Electric Vehicular Applications", *IEEE Trans. On Vehic. Tech.*, vol.60, no.2, pp.433 – 443, Feb. 2011.
- [25] G. Hoogers, *Fuel Cell Technology Handbook*. CRC Press, 2003.
- [26] R.M. Nelms, D.R. Cahela and B.J. Tatarchuk, "Modeling double-layer capacitor behavior using ladder circuits", *IEEE Trans Aerosp Electron Syst*, vol.39, no2, pp.430–438, Apr. 2003.
- [27] R.L. Spyker and R.M. Nelms, "Classical equivalent circuit parameters for a double-layer capacitor". *IEEE Trans Aerosp Electron Syst*, vol.36, no.3, pp. 829–836, Jul. 2000.
- [28] H. El Fadil and F. Giri, "Backstepping based control of PWM DC–DC boost power converters". *In Proc. of the IEEE Int. Symp. on indust. Elect. (ISIE'07)*, Vigo, 4-7 June 2007, pp.395–400.
- [29] H. El Fadil, F. Giri, and H. Ouadi, "Accounting for coils magnetic saturation in controlling DC-DC power converters", *In Proc. of the IEEE Int. Conf. on Contr. Appl. (CCA)*, Munich, 4-6 Oct. 2006, pp.3163–3168.
- [30] J.J. E. Slotine and W. Li. *Applied nonlinear control*. Prentice Hall, 1991.
- [31] P. Thounthong, S. Rael and B. Davat, "Analysis of Supercapacitor as Second Source Based on Fuel Cell Power Generation", *IEEE Trans on Energy Conversion*, vol. 24, no. 1, pp.247 – 255, Mar. 2009.
- [32] M. Ortúzar, J. Moreno, and J. Dixon, "Ultracapacitor-Based Auxiliary Energy System for an Electric Vehicle: Implementation and Evaluation", *IEEE Tran on Indut Elect*, vol. 54, no. 4, pp.2147 – 2156, Aug. 2007.
- [33] A. Hajizadeh and M. A. Golkar, "Control of hybrid fuel cell/energy storage distributed generation system against voltage sag", *Electrical Power and Energy Systems*, vol.32, no.5, pp.488–497, June 2010.
- [34] M. Zeraoulia, M.E.H. Benbouzid and D. Diallo, "Electric Motor Drive Selection Issues for HEV Propulsion Systems: A Comparative Study", *IEEE Tran on Veh Tech*, vol.55, No.6, pp. 1756 – 1764, Nov. 2006.
- [35] X.D. Xue, K.W.E. Cheng and N.C. Cheung, "Selection of electric motor drives for electric vehicles", *In Proc. Of Power Engineering Conference (AUPEC '08)*, 14-17 Dec. 2008, pp.1-6.
- [36] J. Wry, *Electric Vehicle Technology Explained*, John Wiley & Sons, Ltd., 2003.